Environmental Science Nano

PAPER

View Article Online
View Journal | View Issue

Cite this: *Environ. Sci.: Nano*, 2017, 4, 1817

Enhanced biofilm penetration for microbial control by polyvalent phages conjugated with magnetic colloidal nanoparticle clusters (CNCs)†

Ling-Li Li, ‡[a] Pingfeng Yu, ‡[b] Xifan Wang,[b] Sheng-Song Yu,[a] Jacques Mathieu,[b] Han-Qing Yu [a] and Pedro J. J. Alvarez *[b]

Received 10th May 2017,
Accepted 18th July 2017

DOI: 10.1039/c7en00414a

rsc.li/es-nano

Biofilms may shelter pathogenic or other problematic microorganisms that are difficult to eradicate due to hindered penetration of antimicrobial chemicals. Here, we demonstrate the potential for efficient bacterial suppression using polyvalent (broad host-range) phages attached to magnetic colloidal nanoparticle clusters (CNCs) that facilitate biofilm penetration under a relatively small magnetic field (660 gauss). The polyvalent phage PEL1 (*Podoviridae* family) was immobilized onto Fe_3O_4-based magnetic CNCs that had been coated with chitosan (and thus functionalized with amino groups). This facilitated conjugation with phages *via* covalent bonding (*i.e.*, amide linkages) and enabled phage loading, which reached $(5.2 \pm 0.7) \times 10^3$ centers of infection per 1 μg of chitosan-coated CNCs (CS-Fe_3O_4). The plaque formation capability of PEL1–CS-Fe_3O_4 on *Pseudomonas aeruginosa* PA01 and *Escherichia coli* C3000 lawns was significantly higher than that of phages conjugated with similar CNCs that had been functionalized with carboxyl groups (99.1% *vs.* 3.2% Petri dish area of infection). In newly established biofilms formed from these two species on a glass surface, PEL1–CS-Fe_3O_4 removed 88.7 ± 2.8% of the biofilm coverage area after 6 h of treatment. Overall, this conjugation approach could extend the application of phages for microbial control by enhancing their delivery to relatively inaccessible locations within biofilms.

Environmental significance

Biofilms may shelter pathogenic or other problematic microorganisms that are difficult to eradicate due to hindered penetration of antimicrobial chemicals and pose public health concerns. This study demonstrated the potential for efficient bacterial suppression in mixed-species biofilms using broad host-range phages immobilized onto magnetic colloidal nanoparticle clusters (CNCs). The phage–CNC complexes physically disrupt biofilm matrices as they penetrate under a magnetic field, and enhance phage infiltration and delivery to otherwise inaccessible host cells. Compared with free phage treatments, immobilization mitigates phage dilution by the medium to maintain high phage concentrations locally and ensures that phage tail fibers are exposed to the hosts for easier infection. This work suggests that the scope and efficacy of phage applications can be enhanced by magnetic-field-controlled migration with paramagnetic CNCs.

Introduction

Bacterial biofilms are most often composed of multi-species communities embedded in heterogeneous extracellular polymeric substances (EPS).[1] Whereas biofilms have important applications in wastewater treatment and industrial fermentation owing to their enhanced reaction rates and resistance to exogenous stresses,[2,3] they may also shelter pathogenic or problematic microorganisms and pose public health concerns. Additionally, biofilms harboring bacteria involved in metal deterioration can accelerate microbially influenced corrosion, causing billions of dollars in damage annually.[4] Therefore, there is growing interest in novel microbial control approaches that preferentially suppress problematic bacteria without significantly hindering the beneficial functions of biofilms.

Bacteriophages (phages) are viruses that infect and replicate within specific bacterial hosts.[5] Once adhered to a host, lytic phages penetrate the cell membrane, replicate, lyse the host, and release new virions that start the cycle anew. These

[a] *Department of Chemistry, University of Science and Technology of China, Hefei 230026, China*
[b] *Department of Civil and Environmental Engineering, Rice University, Houston, Texas 77005, USA. E-mail: alvarez@rice.edu; Tel: +1 (713) 348 5903*

† Electronic supplementary information (ESI) available: Characterization of polyvalent phage PEL1; synthesis, modification and XRD patterns of magnetic CNCs; data showing a lack of antimicrobial or antiviral effects of different CNCs; data showing the abundance and stability of phages immobilized on CNCs; data showing the efficiency of phage penetration and extent of biofilm disruption by CNCs. See DOI: 10.1039/c7en00414a

‡ Joint first authors.

self-replicating properties, coupled with their ability to exhibit a narrow host range, make phages promising antimicrobial agents for targeted control of problematic bacteria (including biocide- and multidrug-resistant strains).[6,7] Phages can subsequently disappear together with the host, thus avoiding the problem of residual disinfectants.[8,9] Recent studies have shown that polyvalent (broad host-range) phages have the potential for simultaneous targeting of multiple bacterial hosts without impairing total microbial heterotrophic activity.[10] Polyvalent phages, due to their lower adsorption rate constants and broader host range, exhibit higher diffusion within biofilms relative to narrow host-range phages.[11] These traits could be useful for targeting problematic bacteria in complex biofilms, where the presence of multiple species can result in enhanced resistance or virulence[12] – exemplified by the coexistence of *P. aeruginosa* and *Burkholderia cepacia* in biofilms associated with cystic fibrosis patients.[13]

Despite these potential advantages, phage-based biofilm control is limited by two factors: (1) phage dilution due to dispersion in the bulk solution[14] and (2) limited phage penetration into the biofilm matrix.[15,16] To address these challenges (*i.e.*, both increase phage concentration locally and enhance biofilm penetration), we conjugated polyvalent phages with magnetic CNCs. Previous studies with CNCs have shown their potential for controlled drug delivery.[17] CNCs have also been conjugated with phages to bind and facilitate the magnetic separation of bacteria for rapid detection of waterborne pathogens.[18,19]

In this work, we evaluate the efficiency of polyvalent phage–CNC complexes to treat a well-defined two-species biofilm, using *E. coli* C3000 and *P. aeruginosa* PA01 as model target organisms. *E. coli* represents an enteric bacterium commonly associated with fecal pollution and infectious diseases,[20] whereas *P. aeruginosa* exhibits multiple mechanisms of antibiotic resistance and is highly active in biofilm formation.[21] This model biofilm facilitates visualization of how magnetic field manipulation can control the migration of the phage–CNC conjugate. Polyvalent phage PEL1 (isolated from soil) was conjugated with various Fe_3O_4-based CNCs to advance the understanding of how the morphology and surface charge of the CNCs affect phage attachment and infectivity. We show that biofilm penetration by the PEL1–CS-Fe_3O_4 conjugate can be controlled through magnetic field manipulation, and that the infection efficiency of PEL1–CNC complexes is influenced by the surface charge and amino density of the CNCs. This is the first demonstration of polyvalent phage conjugation with CNCs to enhance biofilm penetration and microbial control.

Materials and methods

Bacterial strains, bacteriophage, and cultural conditions

E. coli C3000 (ATCC 15597) and *P. aeruginosa* PA01 (ATCC 15692) were grown in tryptic soy broth (TSB) medium. Polyvalent phage PEL1, which infects both *E. coli* C3000 and *P. aeruginosa* PA01 (Fig. S1†), was isolated using a sequential multi-host isolation method and characterized in terms of growth parameters (Table S1†) and host range (Table S2†) as previously described.[10] All bacterial incubations and viral assays were performed at 30 °C. Bacteriophages were stored at 4 °C in SM buffer (50 mM Tris-HCl [pH 7.5], 0.1 mM NaCl, 8 mM $MgSO_4$, and 0.01% gelatin). The phage titer was expressed as plaque forming units (PFU) per milliliter by using a double-layer plaque assay[10] (tryptone base layer agar as a base layer and tryptone soft agar as a soft agar) in triplicate.

Microscopic analysis of phage particles

Fluorescence microscopy (Olympus IX71) was used to examine polyvalent phages stained with SYBR Gold (Invitrogen).[22] Briefly, 1 ml isolated phage was digested with OmniPur DNase I (Calbiochem, Gibbstown, NJ) at 37 °C for 1 h and then stained with 2.5× SYBR Gold for 10 min in the dark. The phage stock was filtered through a 0.02 μm-pore-size Al_2O_3 Anodisc membrane filter (Whatman, Clifton, NJ) at approximately 20 kPa vacuum. The stained Anodisc filter was mounted on a glass slide with a drop of ProLong Gold Antifade reagent (Invitrogen) and a coverslip.

Synthesis and characterization of Fe_3O_4-based magnetic CNCs

Fe_3O_4 CNCs, chitosan-coated Fe_3O_4 CNCs (CS-Fe_3O_4), core–shell Fe_3O_4@SiO_2 CNCs, amino group-modified Fe_3O_4@SiO_2 CNCs (Fe_3O_4@SiO_2–NH_2), and carboxyl group-modified Fe_3O_4@SiO_2 CNCs (Fe_3O_4@SiO_2–COOH) were used for phage conjugation and to investigate the effect of material properties on conjugation efficiency. Briefly, Fe_3O_4 CNCs were synthesized using a solvothermal reaction with sodium acetate and $FeCl_3{\cdot}6H_2O$.[23] Fe_3O_4@SiO_2 CNCs were prepared by a versatile solution sol–gel method.[24] Amino groups were introduced onto the surface of Fe_3O_4@SiO_2 CNCs by a conventional sol–gel reaction with (3-aminopropyl)triethoxysilane (APTES) as a modifying agent.[25] Carboxyl groups were then functionalized by a chemical reaction between the amino groups and succinic anhydride. Chitosan-coated Fe_3O_4 (CS-Fe_3O_4) CNCs were synthesized using $FeCl_3{\cdot}6H_2O$, NaOAc, chitosan, and 1-ethenylpyrrolidin-2-one (PVP) *via* a versatile solvothermal reaction to obtain magnetic CNCs with porosity and high protonation of amino groups.[26] Details on CNC synthesis and modification are available in the ESI.†

Material samples were dispersed in DI water and dried onto lacey carbon copper grids for TEM analysis. Specimens were observed with a JEOL 2010 transmission electron microscope at 200 kV and size distributions of CNCs were estimated based on 100 particles under TEM. The surface zeta potentials of all CNCs were determined in phosphate buffer (PBS, pH = 7.2) at 20 °C using a Nanosized Zetasizer instrument (Malvern Instruments Co., UK). The crystalline properties and phase identification were characterized by XRD (Fig. S2†), using a Japan Rigaku DMax-γA rotation anode X-ray diffractometer equipped with graphite-monochromatized Cu K_α

radiation. The attenuated total reflectance Fourier transform infrared (ATR-FTIR) spectra were recorded on a Vertex 70 FTIR spectrometer (Bruker Co., Germany) equipped with a deuterated triglycine sulfate detector.

Polyvalent phage conjugation with magnetic CNCs

Polyvalent phage PEL1–MM complexes were prepared by the reaction between carboxylic and amino groups under activation by *N*-hydroxysuccinimide (NHS) and 1-ethyl-3-(3-(dimethylamino)propyl)carbodiimide hydrochloride (EDC).[18,27] Accordingly, CNCs (1 mg) were dispersed in 1 mL DI water, mixed with EDC (200 μL, 20 mg mL^{-1}) and NHS (100 μL, 20 mg mL^{-1}) by ultrasonication for 30 min at 25 °C. Then, PEL1 phage stock (200 μL, 6×10^9 PFU mL^{-1}) was mixed with the activated CNCs and rotated at 30 rpm overnight at 4 °C. Next, PEL1–CNCs were separated, washed to remove excess PEL1 phage, and dispersed in 1 mL PBS buffer with 0.05% BSA for 2 h at 4 °C to block residual reactive sites.

The number of phages immobilized onto CNCs was quantified by double-layer plaque assay as the difference between the initial phage amount and the total number of free phages remaining in the conjugation plus washing solutions (see the ESI† for sample calculations). During the washing step (repeated three times), PEL1–CNC complexes were vortexed at 240 rpm for 10 seconds and precipitated under a magnetic field to detach loosely bound phages. Phage stock was also cultivated with EDC and NHS (but no CNCs) as a control to estimate the antiviral effect of these chemicals. Phage stock cultivated with CNCs alone (*i.e.*, no EDC or NHS to avoid stimulating conjugation) was used as an additional control to assess the effect of various CNCs on phage adsorption and viability. The amount of phages adsorbed to the CNC phages was similarly calculated as the difference between the initial phage amount and the total number of remaining free phages in the conjugation plus washing solutions. Following the separation and washing steps, the PEL1–CNCs were stored in 1 mL PBS buffer at 4 °C. The PEL1–CNC complexes were further confirmed by TEM using a JEOL 2010 and fluorescence microscopy (using SYBR Gold-stained phages).

Infective activity of PEL1–CNC complexes

The plaque formation capability of PEL1–CNC complexes was quantified in triplicate by double-layer plaque assay using mixed bacteria (OD_{600} = 0.5, equal ratio of *P. aeruginosa* and *E. coli*). The plates were incubated at 30 °C for 12 hours. MATLAB was used to estimate the fractional area of plaque formed on the bacterial lawn. The infectivity of PEL1–CNCs towards bacterial hosts was further confirmed by scanning electron microscopy[28] using a JEOL 6500 instrument. The samples were fixed with 3% glutaraldehyde (wt/vol) in PBS buffer followed by gradient ethanol dehydration.[29] The samples were placed on a carbon tape-pasted stub and then sputter-coated with a ~5 nm gold film under vacuum (Denton Desk V sputter system).

Bacterial challenge tests under biofilm conditions

96-well special optical plates were used to cultivate the mixed biofilm which contained 120 μL M63 buffer, inoculated with overnight cultures of *P. aeruginosa* and *E. coli* at a final cell density of OD_{600} = 0.1 each. After 24 h of cultivation by horizontally shaking at 100 rpm and 30 °C, the wells which showed biofilm growth were gently washed 3 times with PBS buffer to remove the unattached cells, and 160 μL PBS buffer with 10 mM $MgSO_4$ was then added. Phage PEL1 only, a mixture of PEL1 and CS-Fe_3O_4, or a PEL1–CS-Fe_3O_4 complex was added to a final concentration of 4×10^5 PFU mL^{-1}. CS-Fe_3O_4 was also added to assess the effect of mechanical disruption on biofilm integrity. After 6 h of treatment in a static state, the CNCs, suspended cells and cell debris were removed and the residual biofilms were stained with propidium iodide (PI) and SYTO9 from a LIVE/DEAD BacLight kit (Invitrogen AG, Basel, Switzerland) according to the manufacturer's instructions. The stained live and dead bacteria were examined under fluorescence microscopy.

Transport of PEL1–CNC complexes with magnetic orientation control

Transport of conjugated phage PEL1 was conducted in a double-layer plate with *P. aeruginosa* and *E. coli* embedded in the soft layer. A thin film of SM buffer was added on top of the soft layer and the PEL1–CNC complexes were loaded in the center of the plate. A magnetic cylinder (K&J Magnetics, 660 gauss) was used to control the movement of the PEL1–CNCs. After air-drying in the hood for 10 min, the plates were incubated at 30 °C overnight to allow the conjugated phages to form clear spots on the bacterial lawn. Penetration of conjugated phages through 0.1% agarose was performed on microscope slides with magnetic orientation control (660 gauss). The SYBR Gold-stained phages were conjugated with CNCs to render a fluorescence signal on the PEL1–CNC complexes. The slides were observed with a fluorescence microscope after the gel was air-dried in the dark.

Statistical analysis

Student's *T*-test (unpaired, two-tailed) was used to determine the significance of the differences between treatments. Differences were significant at the 95% level ($p < 0.05$).

Results and discussion

Polyvalent phage PEL1 was covalently immobilized on CNCs with high efficiency

Using a sequential multiple-host isolation approach,[10] phage PEL1 was isolated with the ability to infect *E. coli* C3000 and *P. aeruginosa* PA01 and significantly suppress their growth (Fig. S1†). Host range tests showed that phage PEL1 can infect additional (but not all tested) *E. coli* and *P. aeruginosa* strains (Table S2†). Based on its short tail and non-enveloped morphology observed under electron microscopy (Fig. 1A), phage PEL1 belongs to the family of *Podoviridae*.

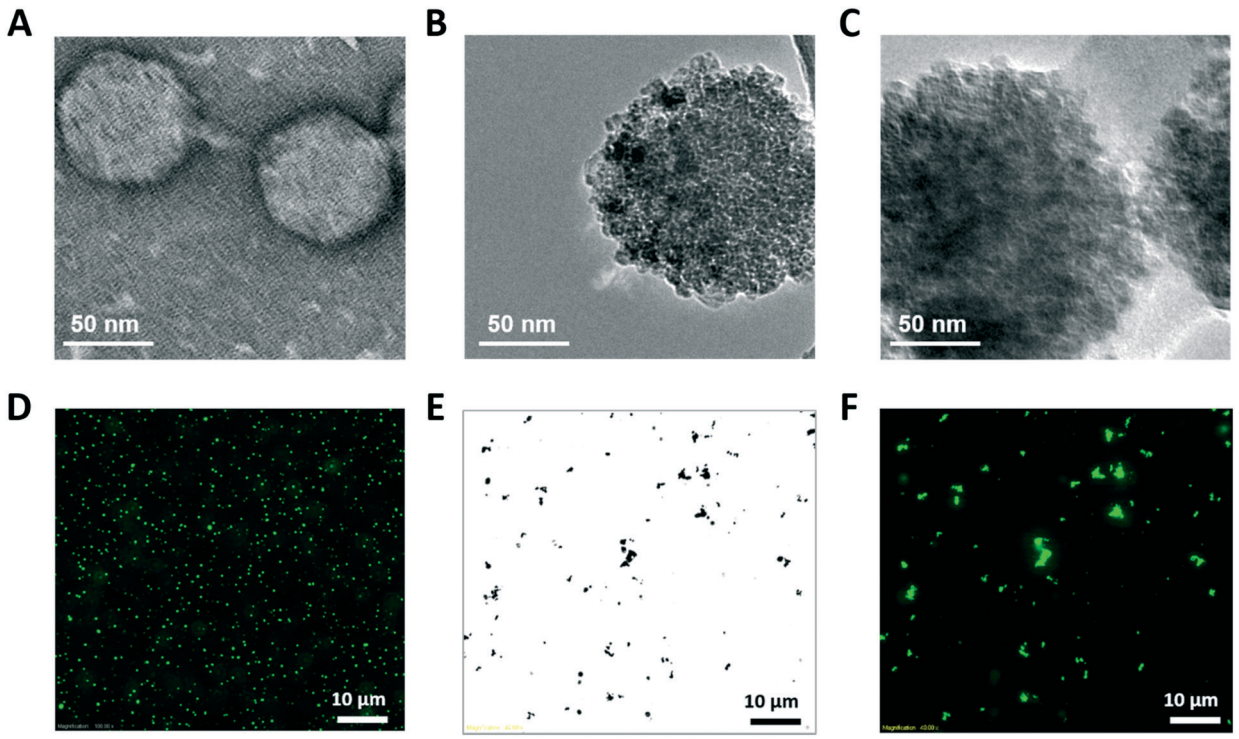

Fig. 1 Microscopic characterization of phage conjugation with magnetic CNCs. Transmission electron microscopy images of (A) uranyl acetate negatively stained polyvalent phage PEL1, (B) newly synthesized CS-coated Fe_3O_4, and (C) polyvalent phage PEL1-conjugated CS-Fe_3O_4; effective phage conjugation is corroborated by fluorescence images, which depict (D) SYBR gold-stained polyvalent phage PEL1, (F) polyvalent phage PEL1 conjugated to CS-Fe_3O_4, and (E) the corresponding light micrograph depicting the CS-Fe_3O_4.

Spherical CS-Fe_3O_4 CNCs with a rough surface and mesoporous structure (Fig. 1B) were used to immobilize phage PEL1 following an EDC/NHS covalent coupling procedure. After conjugation with PEL1, the CNCs appeared wrapped, suggesting successful surface coating (Fig. 1C). Phage conjugation was confirmed by fluorescence images (Fig. 1D to F). CS-Fe_3O_4 displayed strong fluorescence (Fig. 1F) only after the conjugation with phage PEL1, which was pre-stained with SYBR Gold (Fig. 1D). Given the initial phage number of 1.2×10^9 PFU, the residual $(9.0 \pm 0.2) \times 10^8$ PFU free phage after conjugation, and the $(1.4 \pm 0.1) \times 10^8$ PFU phage inactivated by EDC and NHS, the total phage immobilized onto 1 mg CS-Fe_3O_4 was $(1.6 \pm 0.2) \times 10^8$ PFU ($n = 3$). Control tests showed that non-covalent associations of phages with CNCs were relatively small compared to conjugation (Fig. S3†) since adsorbed phages could be easily recovered by CNC washing. Furthermore, CNCs did not exert a significant adverse effect on phage viability (Fig. S4A†).

The PEL1–CS-Fe_3O_4 complexes retained broad infectious activity as demonstrated by plaque assays (Fig. 2A) and

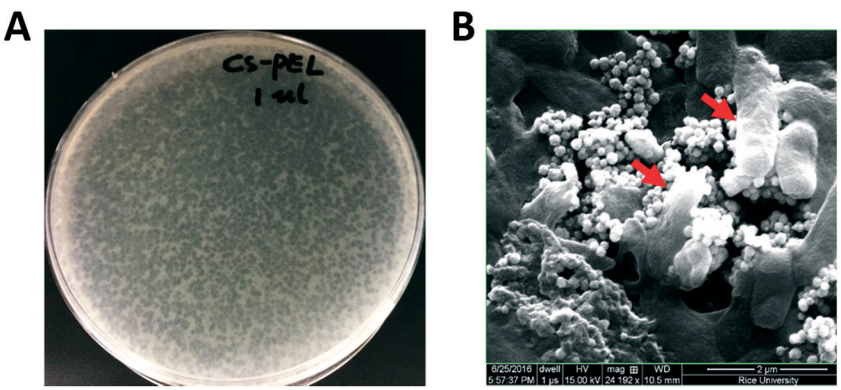

Fig. 2 Infective activity of phage PEL1 after conjugation with chitosan-coated Fe_3O_4. Phage plaques formed on a lawn of mixed bacteria (*P. aeruginosa* and *E. coli*) infected with 1.0 μg PEL1–CS-Fe_3O_4 (A); SEM image of mixed bacteria infected with PEL1–CS-Fe_3O_4 (B), PEL1–CS-Fe_3O_4 adsorbed to intact bacteria (red arrows). Scale bar represents 2 μm.

electron microscopic analysis (Fig. 2B). Specifically, the two-species bacterial lawn was lysed by PEL1–CS-Fe_3O_4, which confirmed its capability to infect both bacterial hosts. Each PEL1–CS-Fe_3O_4 complex served as a center of infection (COI) and would form a single plaque on the bacterial lawn. Serial dilution and plating assays demonstrated that the plaque formation capability of 1.0 mg PEL1–CS-Fe_3O_4 was about (5.2 ± 0.7) × 10^6 COI on the two-species bacterial lawn (Fig. S5A†). This corresponds to an average of 30 ± 8 active phages loaded onto a CNC, and therefore one phage–CNC complex formed a relatively larger plaque compared with one free phage (5.7 ± 0.9 *vs.* 2.6 ± 0.6 mm, n = 50) (Fig. S5B†). For the following biofilm treatment, the equivalent titer of immobilized PEL1 was used as the control group.

Covalent immobilization of bacteriophages on magnetic particles is stable and irreversible (Fig. S3†), and previous studies have shown that direct covalent coupling with EDC–NHS produces the highest coverage of phages on the superparamagnetic particles, even compared with antigen-specific interactions.[30] Thus, CNC–phage complexes hold great promise for achieving targeted contact[31] while enhancing biofilm penetration.

CNC surface amination contributed to efficient conjugation and microbial control

Several magnetic CNCs (Fig. 3) were tested for their ability to graft a high density of active phages and facilitate bacterial infection after conjugation. TEM images show that the synthesized naked Fe_3O_4 particles (50–100 nm) tended to agglomerate (Fig. 3A). Fe_3O_4@SiO_2–NH_2, which also underwent some agglomeration prior to coating with a 20 to 30 nm silica shell, exhibited a broader size distribution (100–220 nm) (Fig. 3B). In contrast, CS-Fe_3O_4 formed stable, dispersed particles with a typical smaller size of 80 to 140 nm (Fig. 3C), which is conducive to a larger specific surface area and more COIs after conjugation with phages.

Conjugated CNCs with amino modification (PEL1–CS-Fe_3O_4 and Fe_3O_4@SiO_2–NH_2) had a higher phage loading and displayed significantly ($p < 0.05$) higher infection ability compared with those conjugated with carboxyl-modified CNCs (PEL1–Fe_3O_4@SiO_2–COOH) (Fig. 4). Specifically, PEL1–CS-Fe_3O_4 loaded 1.6 ± 0.2 × 10^8 PFU mg^{-1}, compared to 1.1 ± 0.2 × 10^8 PFU mg^{-1} for PEL1–Fe_3O_4@SiO_2–NH_2, 8.6 ± 0.8 × 10^7 PFU mg^{-1} for PEL1–Fe_3O_4@SiO_2, 7.4 ± 0.5 × 10^7 PFU mg^{-1} for PEL1–Fe_3O_4, and 5.7 ± 0.6 × 10^7 PFU mg^{-1} for PEL1–Fe_3O_4@SiO_2–COOH (n = 3). Correspondingly, PEL1–CS-Fe_3O_4 had the best infection ability with a plaque area fraction of 99.1 ± 0.6%, while less plaque formed in plates infected with PEL1–Fe_3O_4@SiO_2–NH_2 (50.4 ± 2.7%), PEL1–Fe_3O_4@SiO_2 (30.4 ± 1.9%), PEL1–Fe_3O_4 (12.1 ± 1.4%), and PEL1–Fe_3O_4@SiO_2–COOH (3.2 ± 0.4%) (Fig. 3). The CNCs themselves (without phages) were not bactericidal and did not contribute to plaque formation (Fig. S4B†).

Directional immobilization of phage particles *via* their heads is needed to ensure that tail fibers (which are

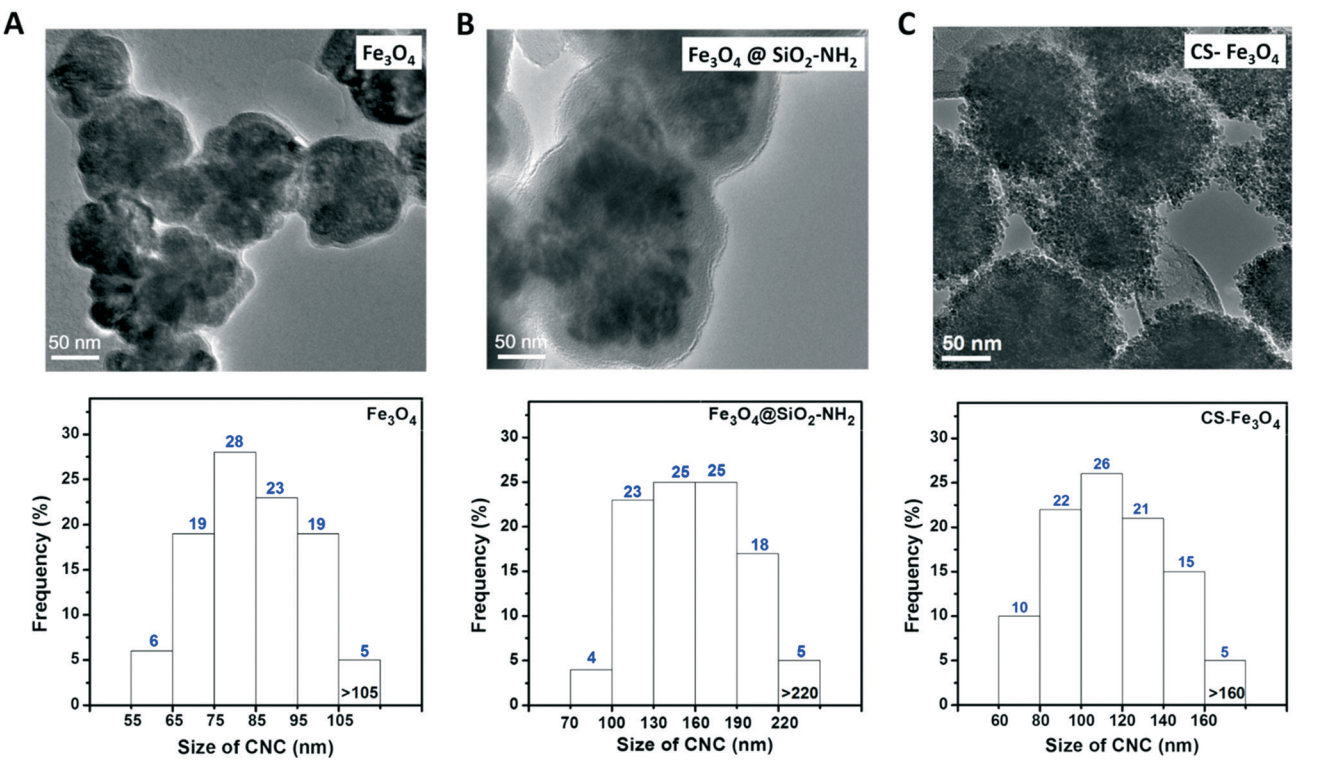

Fig. 3 Morphology and size distribution of Fe_3O_4 CNCs (A), Fe_3O_4@SiO_2–NH_2 CNCs (B), and chitosan-coated Fe_3O_4 (CS-Fe_3O_4) CNCs (C). Fe_3O_4@SiO_2 CNCs and Fe_3O_4@SiO_2–COOH CNCs showed similar morphology and size distribution to Fe_3O_4@SiO_2–NH_2 CNCs. Size distributions of CNCs were obtained from 100 clusters observed under TEM.

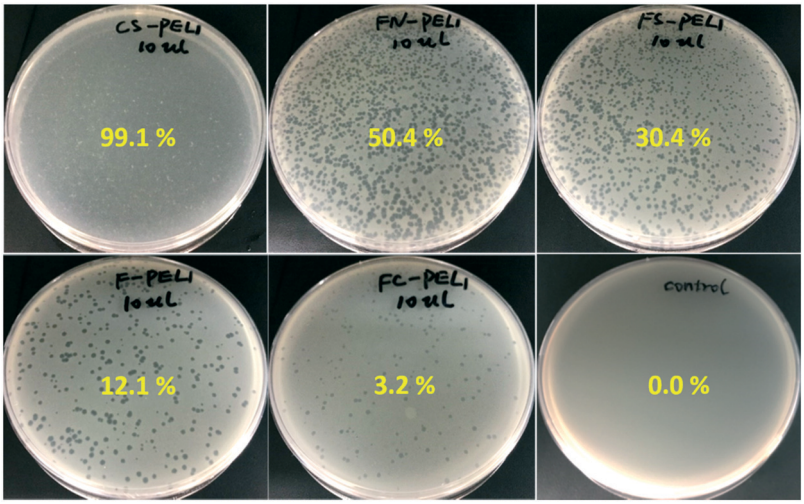

Fig. 4 Plaque formation capabilities of PEL1 immobilized on different CNCs. Phage plaque formation area after 12 h of treatment with 10 μg of PEL1-conjugated CS-Fe_3O_4 (CS–PEL1), PEL1-conjugated Fe_3O_4 CNCs (F–PEL1), PEL1-conjugated Fe_3O_4@SiO_2 core–shell CNCs (FS–PEL1), PEL1-conjugated Fe_3O_4@SiO_2–NH_2 CNCs (FN–PEL1), and PEL1-conjugated Fe_3O_4@SiO_2–COOH CNCs (FC–PEL1) and without treatment (control). Percentages (means of triplicates) represent the fraction of plaque formation area.

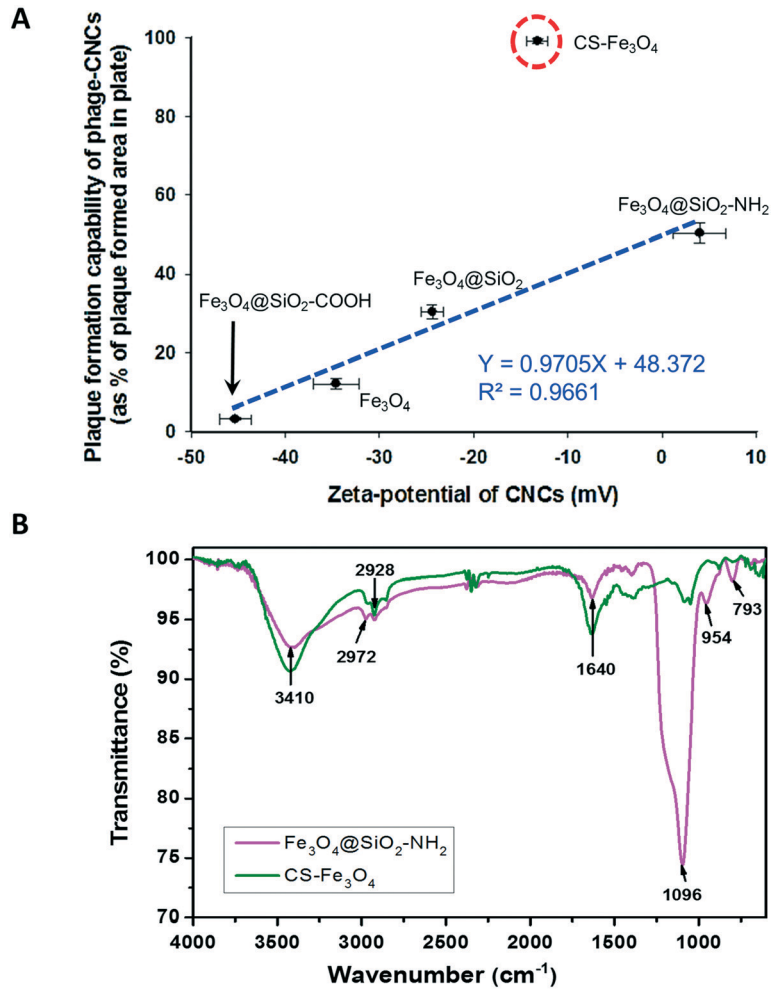

Fig. 5 Effect of CNC zeta potential on plaque formation capability. Panel (A) shows that the zeta potential of CNCs is positively correlated with the antimicrobial effect after phage conjugation (R^2 = 0.966). CS-Fe_3O_4 was an outlier possibly due to its high amino group density that facilitates higher phage loading with proper orientation for enhanced infectivity. Error bars represent the standard deviation of triplicate measurements. Panel (B) compares the FT-IR spectra of Fe_3O_4@SiO_2–NH_2 and CS-Fe_3O_4, highlighting the higher amino group density of the latter.

responsible for host recognition) are exposed to the host.[32] It has been reported that the net charge on most viruses is negative, and the capsids acquire a negative overall charge above pH 4,[33] while another earlier study suggested that the head of T7 phage (*Podoviridae* family) was responsible for the overall negative charge and the tail fibers could be positively charged.[34] Therefore, increased amino group density on the particle surface may not only provide more covalent binding sites for the carboxylic groups on the phage head (increasing phage density),[27] but also orient the tail fibers outwards to facilitate host recognition and infection efficiency.

Coating the Fe_3O_4 CNCs with SiO_2 shells increased the zeta potential from −34.6 to −24.4 mV. The zeta potential further increased to +4.0 mV when the CNCs were coated with APTES (Fe_3O_4@SiO_2–NH_2), and decreased to −45.3 mV after coating with carboxyl groups (Fe_3O_4@SiO_2–COOH) that were conjugated to the amino group, which neutralized the positive charges. Plaque formation tests indicate a high correlation between zeta potential and phage immobilization, with higher infection efficiency corresponding to the higher zeta potential (Fig. 5A, R^2 = 0.966). Nevertheless, PEL1–CS-Fe_3O_4 resulted in a much higher infectivity than predicted by this positive correlation (Fig. 5A). Apparently, the amino groups on PEL1–CS-Fe_3O_4 facilitated phage conjugation with proper orientation (*i.e.*, with tail fibers exposed to the host as illustrated in the graphical abstract), which enhanced infectivity. For example, the number of phages immobilized onto PEL1–CS-Fe_3O_4 was about 2.8-fold higher than that immobilized onto PEL1–Fe_3O_4@SiO_2–COOH, while its plaque area formed was about 31-fold higher (Fig. 4). This reflects the importance of proper orientation when phages are conjugated with CNCs.

Polyvalent phage PEL1 conjugated with CS-Fe_3O_4 showed significantly higher infection efficiency than PEL1–Fe_3O_4@SiO_2–NH_2 ($p < 0.05$), which had a higher positive charge (+4.0 mV *vs.* −13.2 mV) and larger specific surface area (86 m^2 g^{-1} *vs.* 71 m^2 g^{-1}). One possible explanation is that CS-Fe_3O_4 contained a higher density of amino groups than Fe_3O_4@SiO_2–NH_2, and thus could load more properly oriented phages on its surface. Therefore, FTIR spectroscopy was used to compare the amino group density between CS-Fe_3O_4 and Fe_3O_4@SiO_2–NH_2 (Fig. 5B). Due to its SiO_2 shell, Fe_3O_4@SiO_2–NH_2 exhibited the characteristic vibration peaks of SiO_2 (793 cm^{-1}), Si–OH (954 cm^{-1}) and Si–O–Si (1096 cm^{-1}).[26] The absorption bands at 2972 and 2928 cm^{-1} assigned to the stretching vibration of the C–H bond of the propylamine group, which proves the successful grafting of APTES on silica-coated magnetic CNCs (Fe_3O_4@SiO_2–NH_2)[35] and of chitosan on magnetic CNCs (CS-Fe_3O_4).[36] Compared with Fe_3O_4@SiO_2–NH_2, CS-Fe_3O_4 exhibited much stronger characteristic absorption peaks of the primary amine (–NH_2); one overlaps with the –OH band at 3410 cm^{-1}, and the second is visible at 1640 cm^{-1}.[26] Based on the above results, PEL1–CS-Fe_3O_4 was chosen for further experiments.

PEL1–CS-Fe_3O_4 complexes exhibited higher biofilm suppression than free phages

For bacterial control, the conventional phage therapy approach is to apply lytic virulent phages directly on the targeted bacteria.[7] Approaches to increase microbial control efficacy include (1) applying a cocktail of different phages with overlapping host ranges or polyvalent phages to deal with single or dual species biofilms,[37] (2) combining phages with chemical disinfection methods to enhance biofilm control,[38] and (3) combining antibiotic agents (*i.e.*, rifampicin) with phage treatment to remove pathogenic (*Staphylococcus aureus*) biofilms.[39] Nevertheless, insufficient phage penetration into deeper layers of the biofilm is still a major limiting factor.[15,40] This limitation can be significantly ameliorated by magnetic control.

For example, in the free phage-only treatment, the biofilm coverage area decreased by 35.5 ± 6.6%, and the dead/live ratio (45.9 ± 12.1%) increased relative to the control group (11.8 ± 2.1%) (Fig. 6B). However, since dead cells may hinder PEL1 diffusion in biofilms and protect otherwise vulnerable bacteria,[41] there was a need for enhanced phage penetration and treatment efficacy. Due to mainly physical disruption, the CS-Fe_3O_4-only treatment achieved a total biofilm coverage removal of 10.2 ± 3.3% with a dead/live ratio of 10.2 ± 0.5% in the remaining biofilm. The diffusion of CNCs through the biofilm disrupted the biofilm structure and facilitated phage infection. Accordingly, the combination of free phages and CS-Fe_3O_4 resulted in 70.8 ± 4.2% biofilm removal and a 36.4 ± 5.2% dead/live ratio in the remaining biofilms. PEL1–CS-Fe_3O_4 complexes showed an even higher efficacy of biofilm coverage removal (88.7 ± 2.8%), suggesting that phage immobilization can enhance infection due to higher local phage concentrations and effective penetration and directional adsorption. In contrast, free phages are dispersed in the solution and do not effectively penetrate the biofilm by diffusion alone (Fig. S6†).

Whereas the magnetic properties of the phage–CNC complex clearly enhanced biofilm penetration and physical disruption under a magnetic field (Fig. S7†), immobilization of multiple phages on a single CNC is also conducive to higher localized phage concentrations reaching the biofilm. This increases the likelihood of an effective phage–host collision, as does the exposed-tail orientation of the immobilized phages.

The emergence of phage resistance is a challenge for the application of phages in disease control. Conjugation with CNCs and the resulting higher local phage concentrations may not prevent phage resistance, but this approach would disrupt the biofilm matrix faster and incur fitness costs to the surviving bacteriophage-insensitive mutants, which facilitates further microbial control (*e.g.*, reduced growth rate,[9] decreased antibiotic resistance,[42] or less virulence[43]). Possible strategies to avoid or attenuate phage resistance include immobilizing phage cocktails onto CNCs[9] and combining phages with antibiotics.[44] In theory, the performance of phage–CNC complexes could be further improved by using

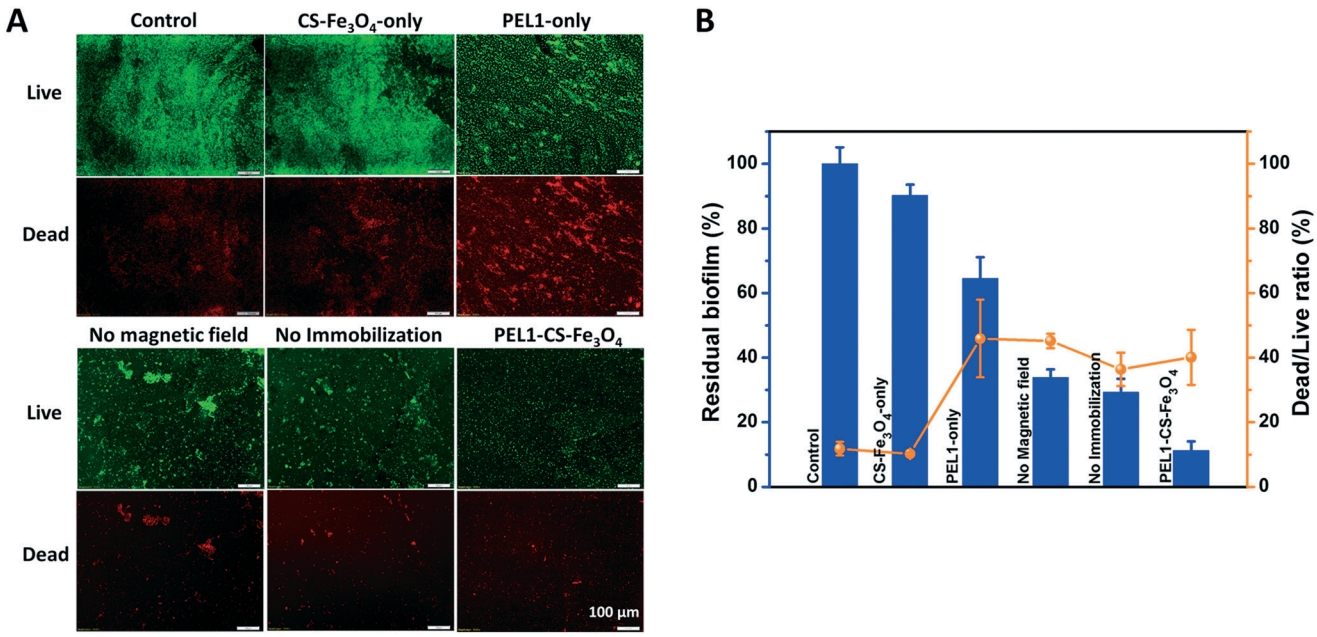

Fig. 6 Fluorescence microscopic analysis of mixed biofilm disruption. (A) Comparison of the remaining biofilm determined by a live (green)/dead (red) assay without any treatment (control), with free phage treatment only (PEL1-only) and material treatment only (CS-Fe_3O_4-only), with both free phage and materials added (no immobilization), and with PEL1–CNC complexes in the presence (PEL1–CS-Fe_3O_4) or absence (no magnetic field) of a magnetic field. (B) Histograms showing the fraction of the remaining biofilm (area of both live and dead bacteria), and the coverage of control was defined as 100%. Enumeration assays were performed three times, and the error bars denote mean ± one standard deviation.

genetically modified phages that disrupt bacterial biofilms by expressing EPS depolymerase[45] and/or quorum-quenching enzymes.[46] However, further research that includes consideration of the fate of such cloned phages and the potential for unintended consequences would be needed to assess their feasibility.

Enhanced biofilm penetration and directional control of the phage–CNC complex were achieved by magnetic-field-controlled migration

Well-established biofilms show a fractal and spatial structure of populations and a complex matrix that is difficult for free phages to penetrate, mainly due to static hindrance and non-specific adsorption.[11] This may compromise the efficacy of phage-based microbial control. However, CNC-conjugated polyvalent phages could help overcome these limitations by enhancing penetration and physical disruption of biofilms and facilitating directional control, as illustrated by the induced horizontal migration (Fig. 7). Specifically, using a relatively weak (660 gauss) magnetic field, we manipulated the horizontal transport of PEL1–CNC conjugates within a bacterial lawn containing both *E. coli* and *P. aeruginosa*. The plates without a magnetic field formed round plaques on the bacterial lawn, while the plates with an oriented magnetic field formed arrowhead-shaped plaques (Fig. 7A). Agarose gel can, to some extent, simulate the biofilm conditions,[47] and the conjugated phages penetrated through the agarose gel with a

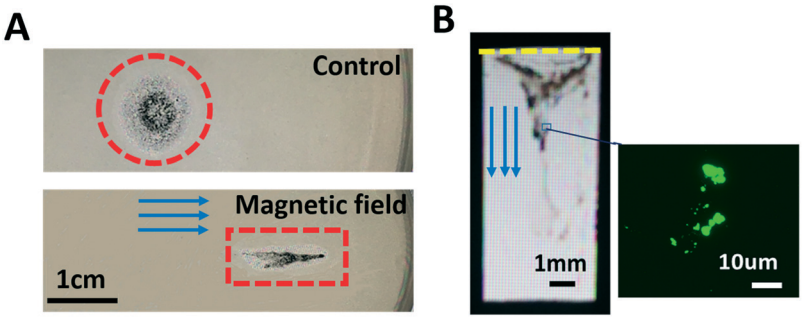

Fig. 7 Horizontal transport and vertical penetration of PEL1–CS-Fe_3O_4 complexes under a magnetic field. Horizontal transport of conjugated phage PEL1 was conducted on the soft layer containing *P. aeruginosa* and *E. coli* (A). The red circle or rectangle shows host lysis. The penetration of conjugated PEL1 was performed in 0.1% agarose gel, followed by SYBR Gold staining (B). The yellow line shows the initial location of conjugated phages, and the blue arrows represent the direction of the magnetic field.

magnetic field (Fig. 7B), consistent with the significantly enhanced biofilm removal efficacy of the PEL1–CS-Fe_3O_4 complex after magnetic orientation control (Fig. 6).

Conclusions

Diffusion of free phages through biofilms is often limited by the presence of EPS matrices,[15] bacterial lysis debris[41] and phage-resistant bacteria.[48] Here, we demonstrate that magnetic CNCs can be used for phage immobilization to enhance their penetration and microbial control in biofilms that are generally resistant to chemical disinfection. The phage–CNC complexes physically disrupt biofilm matrices as they penetrate under a magnetic field, and enhance phage infiltration and delivery to otherwise inaccessible host cells. Compared with phage-only treatments, immobilization mitigates phage dilution by the medium to maintain high phage concentrations locally and ensures that phage tail fibers are exposed to the hosts for easier infection.

This work suggests that the scope and efficacy of phage applications can be enhanced by magnetic-field-controlled migration with paramagnetic CNCs, offering opportunities for more accurate targeting of problematic bacteria in complex biofilms. Nevertheless, further research is needed with well-established, complex biofilms to enhance practical applications, including quantitative characterization of dose–response patterns for various phage–CNC complexes, treatment time and frequency optimization (including potential rotation of phage cocktails to minimize resistance development), and effects of environmental factors on treatment efficiency.

Acknowledgements

This study was supported by NSF PIRE grant (OISE-1545756) and by the NSF ERC on Nanotechnology-Enabled Water Treatment (EEC-1449500). Ling-li Li received partial financial support from the China Scholarship Council. We gratefully acknowledged Danning Zhang for his work on material characterization.

References

1 R. E. Steinberger and P. A. Holden, *Biofilms*, 2004, **1**, 37–47.
2 E. Syron and E. Casey, *Environ. Sci. Technol.*, 2008, **42**, 1833–1844.
3 N. Qureshi, B. A. Annous, T. C. Ezeji, P. Karcher and I. S. Maddox, *Microb. Cell Fact.*, 2005, **4**, 24.
4 H. Wang, C. Hu, X. Hu, M. Yang and J. Qu, *Water Res.*, 2012, **46**, 1070–1078.
5 O. Bergh, K. Y. Borsheim, G. Bratbak and M. Heldal, *Nature*, 1989, **340**, 467–468.
6 T. M. Viertel, K. Ritter and H.-P. Horz, *J. Antimicrob. Chemother.*, 2014, **69**, 2326–2336.
7 A. S. Bhattacharjee, J. Choi, A. M. Motlagh, S. T. Mukherji and R. Goel, *Biotechnol. Bioeng.*, 2015, **112**, 1644–1654.
8 S. A. A. Jassim and R. G. Limoges, *World J. Microbiol. Biotechnol.*, 2014, **30**, 2153–2170.
9 P. Yu, J. Mathieu, G. W. Lu, N. Gabiatti and P. J. Alvarez, *Environ. Sci. Technol. Lett.*, 2017, **4**, 137–142.
10 P. Yu, J. Mathieu, M. Li, Z. Dai and P. J. J. Alvarez, *Appl. Environ. Microbiol.*, 2016, **82**, 808–815.
11 P. Yu, J. Mathieu, Y. Yang and P. J. J. Alvarez, *Environ. Sci. Technol.*, 2017, **51**, 5270–5278.
12 M. Burmølle, D. Ren, T. Bjarnsholt and S. J. Sørensen, *Trends Microbiol.*, 2014, **22**, 84–91.
13 L. Eberl and B. Tümmler, *Int. J. Med. Microbiol.*, 2004, **294**, 123–131.
14 T. O. Worley-Morse and C. K. Gunsch, *Water Res.*, 2015, **68**, 627–636.
15 R. Briandet, P. Lacroix-Gueu, M. Renault, S. Lecart, T. Meylheuc, E. Bidnenko, K. Steenkeste, M.-N. Bellon-Fontaine and M.-P. Fontaine-Aupart, *Appl. Environ. Microbiol.*, 2008, **74**, 2135–2143.
16 T.-O. Peulen and K. J. Wilkinson, *Environ. Sci. Technol.*, 2011, **45**, 3367–3373.
17 C. T. Yavuz, A. Prakash, J. T. Mayo and V. L. Colvin, *Chem. Eng. Sci.*, 2009, **64**, 2510–2521.
18 J. Chen, S. D. Alcaine, Z. Jiang, V. M. Rotello and S. R. Nugen, *Anal. Chem.*, 2015, **87**, 8977–8984.
19 Z. Wang, D. Wang, A. J. Kinchla, D. A. Sela and S. R. Nugen, *Anal. Bioanal. Chem.*, 2016, **408**, 4169–4178.
20 R. E. Besser, P. M. Griffin and L. Slutsker, *Annu. Rev. Med.*, 1999, **50**, 355.
21 T.-F. Mah, B. Pitts, B. Pellock, G. C. Walker, P. S. Stewart and G. A. O'Toole, *Nature*, 2003, **426**, 306–310.
22 A. Patel, R. T. Noble, J. A. Steele, M. S. Schwalbach, I. Hewson and J. A. Fuhrman, *Nat. Protoc.*, 2007, **2**, 269–276.
23 Y. Tang, S. Liang, S. Yu, N. Gao, J. Zhang, H. Guo and Y. Wang, *Colloids Surf., A*, 2012, **406**, 61–67.
24 Y. Deng, Y. Cai, Z. Sun, J. Liu, C. Liu, J. Wei, W. Li, C. Liu, Y. Wang and D. Zhao, *J. Am. Chem. Soc.*, 2010, **132**, 8466–8473.
25 H. Yang, L. Qin, Y. Wang, B. Zhang, Z. Liu, H. Ma, J. Lu, X. Huang, D. Shi and Z. Hu, *Int. J. Nanomed.*, 2015, **10**, 77–88.
26 M. Shen, W. Jia, C. Lin, G. Fan, Y. Jin, X. Chen and G. Chen, *Nanoscale Res. Lett.*, 2014, **9**, 558.
27 C. S. Jeon, I. Hwang and T. D. Chung, *Adv. Funct. Mater.*, 2013, **23**, 1484–1489.
28 A. Reyes, N. P. Semenkovich, K. Whiteson, F. Rohwer and J. I. Gordon, *Nat. Rev. Microbiol.*, 2012, **10**, 607–617.
29 N. Vyas, R. L. Sammons, O. Addison, H. Dehghani and A. D. Walmsley, *Sci. Rep.*, 2016, **6**, 32694.
30 J. Muzard, M. Platt and G. U. Lee, *Small*, 2012, **8**, 2403–2411.
31 S. Kakar, D. Batra, R. Singh and U. Nautiyal, *Journal of Acute Disease*, 2013, **2**, 1–12.
32 Z. Hosseinidoust, A. L. J. Olsson and N. Tufenkji, *Colloids Surf., B*, 2014, **124**, 2–16.
33 R. Cademartiri, H. Anany, I. Gross, R. Bhayani, M. Griffiths and M. A. Brook, *Biomaterials*, 2010, **31**, 1904–1910.
34 P. Serwer, *J. Chromatogr. B: Biomed. Sci. Appl.*, 1987, **418**, 345–357.
35 E. Dezfoolinezhad, K. Ghodrati and R. Badri, *New J. Chem.*, 2016, **40**, 4575–4587.

36 P. Xuan Nui, N. Tan Phuoc, P. Tuyet Nhung, T. T. Thuy Nga and T. T. Van Thi, *Adv. Nat. Sci.: Nanosci. Nanotechnol.*, 2016, **7**, 045010.
37 W. Fu, T. Forster, O. Mayer, J. J. Curtin, S. M. Lehman and R. M. Donlan, *Antimicrob. Agents Chemother.*, 2010, **54**, 397–404.
38 Y. Zhang and Z. Hu, *Biotechnol. Bioeng.*, 2013, **110**, 286–295.
39 M. Rahman, S. Kim, S. M. Kim, S. Y. Seol and J. Kim, *Biofouling*, 2011, **27**, 1087–1093.
40 S. T. Abedon, *FEMS Microbiol. Lett.*, 2016, **363**, fnv246.
41 S. Heilmann, K. Sneppen and S. Krishna, *Proc. Natl. Acad. Sci. U. S. A.*, 2012, **109**, 12828–12833.
42 B. K. Chan, M. Sistrom, J. E. Wertz, K. E. Kortright, D. Narayan and P. E. Turner, *Sci. Rep.*, 2016, **6**, 26717.
43 M. León and R. Bastías, *Front. Microbiol.*, 2015, **6**, 343.
44 W. N. Chaudhry, J. Concepción-Acevedo, T. Park, S. Andleeb, J. J. Bull and B. R. Levin, *PLoS One*, 2017, **12**, e0168615.
45 T. K. Lu and J. J. Collins, *Proc. Natl. Acad. Sci. U. S. A.*, 2007, **104**, 11197–11202.
46 R. Pei and G. R. Lamas-Samanamud, *Appl. Environ. Microbiol.*, 2014, **80**, 5340–5348.
47 J. Hu, K. Miyanaga and Y. Tanji, *Biotechnol. Prog.*, 2010, **26**, 1213–1221.
48 S. González, L. Fernández, A. B. Campelo, D. Gutiérrez, B. Martínez, A. Rodríguez and P. García, *Appl. Environ. Microbiol.*, 2017, **83**(3), e02821-16.

